Ann. Rev. Nucl. Part. Sci. 1988. 38: 29–66

STATUS OF THE NUCLEAR SHELL MODEL

B. A. Brown

National Superconducting Cyclotron Laboratory, and
Department of Physics and Astronomy, Michigan State University,
East Lansing, Michigan 48824

B. H. Wildenthal

Department of Physics and Astronomy, University of New Mexico,
Albuquerque, New Mexico 87131

CONTENTS

1. INTRODUCTION

Low-lying states of nuclei provide an ideal laboratory in which to study quantum many-body effects. They also provide unique information on the fundamental nature of the strong and weak interactions, provided that the

0163–8998/88/1201–0029$02.00

many-body aspects are sufficiently well understood. The nuclear shell-model provides one of the principal mechanisms for such understanding.

Modern nuclear shell-model calculations incorporate many or all of the multinucleon configurations that arise under the assumption that the valence protons and neutrons of the nucleus simultaneously occupy several different, partially filled, single-particle quantum states. Modern calculations are thus a natural extension of the original nuclear shell-model of Mayer & Jensen (1), which assumed a single configuration for each nuclear level, corresponding to a single nucleon in one single-particle orbit. Current studies require extensive numerical computations in order to translate their underlying concepts into explicit predictions about experimental observations. The increase in available computational facilities during the last several years has made it possible to implement the principles of configuration mixing in the nuclear shell model systematically and with full internal consistency. Significant improvements in the accuracy and comprehensiveness of the theoretical understanding of low-lying nuclear states have been made.

Current research is aimed at a theoretical understanding of the complete spectroscopic characterization of nuclear levels provided by experiments at the impulse approximation level. Such a complete characterization includes predictions of ground-state binding energies; the individual energies of excited states of all spins, parities, and isospins; level densities as a function of excitation energy; the values of the multipole moments of individual levels as revealed by electromagnetic or equivalent probes; the values of the matrix elements between nuclear states of the same mass number corresponding to transitions mediated by weak, electromagnetic, and strong probes with a range of multipolarities; and nucleon-number-changing matrix elements corresponding to the results of transfer-reaction experiments. The values of these matrix elements as functions of excitation energy in the nucleus and of momentum transfer from the probe are also central matters of interest. As we document in this review, significant progress has been taking place in explaining and predicting such phenomena with the shell model. Concurrently, as the model wave functions have been validated against these "conventional" observables, they have also been introduced into the study of more "esoteric" phenomena, such as isospin nonconservation (2), parity nonconservation (3, 4) and double beta decay (5–7).

A program of shell-model research involves selecting the active single-nucleon orbits, along with their allowed configurations and couplings, which should encompass the nuclear phenomena of interest ("defining the model basis space"), and then determining the effective single-particle

potential for, and the effective two-body interaction between, the nucleons considered in the model. With these two "physics" elements of the problem determined, the next step is to carry out the "computational" jobs of constructing the resultant Hamiltonian matrices for the chosen energy operator in the chosen space, of diagonalizing these matrices to obtain eigenvalues and eigenfunctions, and finally, of calculating overlaps of these wave functions. Modern calculations typically are designed to incorporate as many single-nucleon orbits and corresponding "basis states" as computational constraints permit. Even so, many more single-nucleon orbits that may have direct and appreciable effects upon some aspects of the nuclear phenomena of interest must inevitably be truncated from any practical active model space. Hence, results of calculations within the active model space must ultimately be "renormalized" for the effects of excluded configurations in order to yield final agreement with experiment. Renormalizations of the results obtained in the active model space can be calculated from fundamental considerations of neglected configurations and particle degrees of freedom or from macroscopic, heuristic models.

Modern, large-basis shell-model calculations are progressing in several dimensions: (*a*) better methods and models to predict which of the basis states are most important, so that the reach of the active space can be extended without proportional expansion of dimensionalities; (*b*) improved mathematical and computational techniques for projecting angular momentum and setting up and diagonalizing large matrices; (*c*) use of less restrictive, but more discriminating and realistic, assumptions about the effective nucleon-nucleon interaction; and (*d*) theoretical and empirical elucidation of the effects of excluded configurations. These developments are proceeding in parallel with the use of computers that are faster and have larger memories. Advances on these fronts rely on the contributions of many groups working with several different approaches on several different regions of nuclei.

In this review we concentrate on recent results obtained for the sd-shell nuclei. Earlier work in the sd shell has been reviewed elsewhere (8, 9). We briefly summarize work being carried out in other mass regions. All of the sd-shell results presented here produce and use wave functions characterized by good isospin quantum numbers. Experimental binding energies are considered as relative to the ^{16}O closed-shell configuration. Coulomb energy contributions to the experimental binding energies of the ground states are subtracted in an approximate manner (10), and differences in excitation energies of mirror states are averaged or ignored. Recently, charge-dependent and charge-asymmetric interactions have been added to the isospin-conserving interaction discussed below in order to study analogue displacement energies (11), isospin-mixing corrections to

Fermi decays (12), and isospin-forbidden proton and neutron decays (13), for the sd-shell nuclei.

Issues associated with choosing or determining model spaces and effective Hamiltonians are discussed in Section 2, along with some representative results for energies and single-nucleon spectroscopic factors. Correspondences between the magnitudes of experimental and theoretical Gamow-Teller (GT) and magnetic dipole (M1) matrix elements are discussed in Section 3. Because of their relative simplicity and selectivity, the GT and M1 operators provide some of the clearest information about the correctness of the model-space wave functions and about the effects that arise from configurations excluded from the active space. Observables for less simple operators are discussed in subsequent sections, matrix elements of the electric quadrupole (E2) operator in Section 4, and higher-multipole matrix elements and electron scattering form factors in Section 5. Shell-model studies in other mass regions are discussed in Section 6 and prospects and problems for the future in Section 7.

2. MODEL SPACES AND EFFECTIVE HAMILTONIANS

Current shell-model studies of $A = 17$–39 nuclei are characterized by systematic use, for all states of all nuclei in the region and from initial conception through final analysis of the results, of the complete set of basis states that can be generated from the three orbits of the 0d,1s oscillator shell. In this regard they differ from earlier studies of these nuclei (8, 9), in which truncations within the sd-shell space significantly affected the results, either explicitly or implicitly. In this same regard, they differ even more from studies of heavier nuclei, in which untruncated spaces for a full oscillator shell can be utilized for, at most, only a few, few-active-particle nuclei. For these heavier nuclei, the problem of defining a model space that adequately describes the phenomena of interest in a nucleus is a major problem by itself, and the additional problem of defining a space that can describe a range of several nuclei with internal consistency is even more daunting. Theoretical techniques and computer technology have evolved to the level that sd-shell studies can use the untruncated sd-shell space uniformly. Hence, these studies offer a view of the inherent powers of the shell model when intrashell truncation problems are eliminated, and attention can be focused solely upon the issue of the effective interaction. In this regard, the sd-shell studies follow in the footsteps of pioneering work in the 0p shell (14).

Although there are only 24 active m states (i.e. the states specified by

the set of single-particle quantum numbers n, l, j, j_z, and t_z) in the $1s_{1/2}$-$0d_{5/2}$-$0d_{3/2}$ model space, the full-basis dimensions for many-particle states can become quite large; for ^{28}Si the 12-particle state with $M = 0$ for the sum of the j_z quantum numbers and $T_z = 0$ for the sum of the t_z quantum numbers has dimension 93,710 in the m scheme, and in the J-T scheme the 12-particle $J = 3$, $T = 1$ configuration has dimension 6706. These dimensions are practical, if not trivial, for current computation facilities. The computer times required to deal with such cases correspond roughly to the order of a VAX-780 day or a Cray hour. For such large matrix dimensions it is essential to use the Lanczos algorithm to obtain the eigenfunctions (15). Many of the large full-basis calculations for sd-shell nuclei were first carried out with the Glasgow m-scheme code in which Lanczos diagonalization was pioneered (15). The calculations presented here are obtained principally with the Michigan State University version of the Rochester–Oak Ridge code, which works in spaces of specified J and T and also employs Lanczos diagonalization (10, 16).

In a spherical shell-model basis the energies of large-dimensioned sd-shell states converge slowly with increasing numbers of configurations. This is illustrated in Figure 1, which shows the binding energies of the ^{28}Si spectrum for the $(d_{5/2})^{12}(s_{1/2})^0(d_{3/2})^0$ "closed-subshell" configuration (excitation order 0) and for a succession of configuration spaces corresponding to increasing numbers of excitations from the $d_{5/2}$ to the $s_{1/2}$ and $d_{3/2}$ orbitals (excitation order 1 to 12). The same interaction (the W interaction discussed below) has been used for each calculation. The ground-state m-scheme dimension (i.e. the total number of states in each spectrum) is also given, and the low-lying ($T = 0$) states are labeled by their J values. In

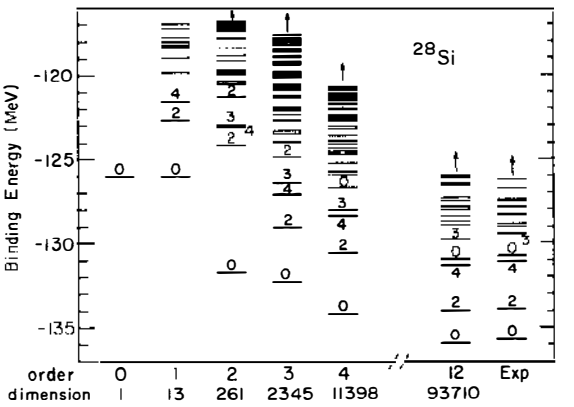

Figure 1 Binding energies of levels in ^{28}Si as a function of the number of excitations from the $d_{5/2}$ orbital (see Section 2).

particular, note the slow convergence in excitation energy for the $J = 2$ and the excited $J = 0$ states. The excitation-order dependence of electromagnetic matrix elements has been studied by Metsch & Glaudemans (17). This slow convergence presumably explains why the evolution of sd-shell model calculations from truncated spaces to uniformly complete spaces yielded simplified, as well as more accurate, results.

Together with specification of the model space, the other primary problem of shell-model calculations is specification of the appropriate effective Hamiltonian operator. Ideally, this could be specified directly by considering experimental nucleon-nucleon scattering data and fundamental theoretical ideas. The free-space nucleon-nucleon interaction would, of course, have to be modified for the effects of excluded configurations if it were to be used in finite model spaces. Much progress has been made in formally deriving such "theoretical" effective interactions from first principles, and they have been qualitatively successful in reproducing nuclear properties (e.g. 18, 19).

For example, a calculation of an sd-shell effective interaction based upon a G-matrix treatment of the nucleon-nucleon data plus core polarization corrections for the effects of excluded configurations has been qualitatively successful in describing the experimental energy level spectra, especially for $A = 18$–21 (e.g. 19–21). However, there are shortcomings to this microscopic, "no-parameter," approach (9). As an example, we show in Figure 2 the spectrum of ^{22}Na based upon the original renormalized G-matrix of Kuo (RK) (21) and the more recent results obtained from the Paris potential and a folded-diagram approach for the core polarization corrections (SKSP4) (19). Such discrepancies between experiment and this class of

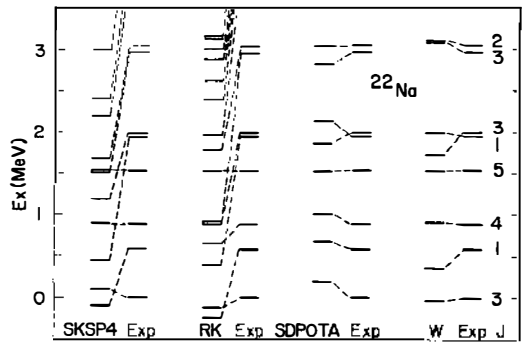

Figure 2 Low-lying excited states of ^{22}Na compared with theoretical calculations discussed in the text. The experimental spectrum is compared with the SKSP4 and RK calculations discussed in Section 2, the W calculation discussed in Section 2.1, and the SDPOTA calculation discussed in Section 2.2.

theoretical results become progressively greater with increasing numbers of active particles because of the nonlinear dependence of the eigenvalues upon the two-body matrix elements.

As an alternative to the direct theoretical calculation of the effective shell-model interaction, phenomenological and empirical considerations can be applied to parameterize an interaction that yields a closer correspondence to experiment. There are many ways of making such a parameterization, ranging from those that depend strongly on a model for the interaction to those that are essentially independent of any such assumptions. The choice of a delta-function interaction is an example of the former class, and the use of the two-body matrix elements themselves as parameters is an example of the latter. It is difficult to judge the relative efficacy of the diverse parameterization methods used in the literature because they typically have been used in isolation from one another and have been applied in different model spaces to different ranges of nuclei. Despite these uncertainties, the model wave functions used most extensively (and successfully) for the analysis of experimental data are generated from empirical parameterizations of the effective interaction (e.g. 8, 9). As described below, with a phenomenological approach it is possible to obtain much improved spectra for ^{22}Na as well as other sd-shell nuclei.

2.1 *Model-Independent Effective Hamiltonians—The W Interaction for sd-Shell Nuclei*

The essence of the "model-independent" approach is to treat the two-body matrix elements and single-particle energies as parameters in a least-squares fit to experimental binding energies and excitation energies. This technique has been applied to the sd shell. Since there are 63 two-body matrix elements for the sd shell, fixing all parameters of the Hamiltonian in this way is a nontrivial task. However, a sustained and systematic attack on the problem has yielded a unified effective interaction for all sd-shell nuclei, obtained in a fit to 447 binding and excitation energies of sd-shell states (mostly states with model dimensions less than about 1000), which yielded an rms deviation of 185 keV (22). (Most states with large dimensions were omitted from the iterative fit calculations in order to save computer time. Subsequent calculations for these cases with the final fitted interaction yielded energies in comparably good or better agreement with experiment; see Figure 3.) The working parameters of this fit were actually the 47 best-determined linear combinations of two-body matrix elements. The 19 least-well-determined linear combinations were fixed to correspond to values of Kuo's matrix elements (21). We refer to the two-body matrix elements obtained from this fit as the W interaction.

Over the mass region $A = 16$–40 one should expect some variation in

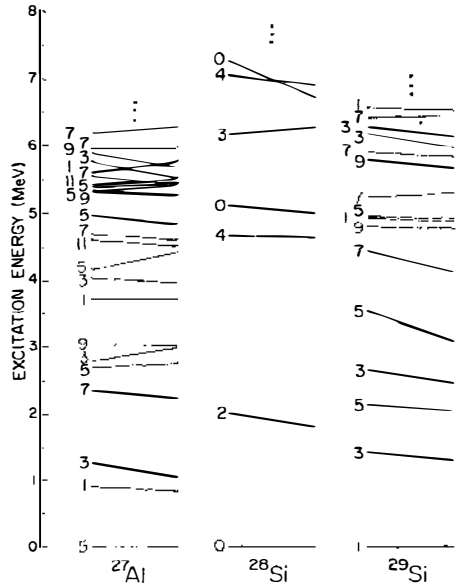

Figure 3 Experimental (*right edge*) vs theoretical (*left edge*) energy levels of ^{27}Al, ^{28}Si, and ^{29}Si. The calculations were obtained with the W interaction discussed in Section 2.1.

the values of the two-body matrix elements. For example, with a delta-function interaction and harmonic oscillator radial wave functions with $\hbar\omega = 41A^{-1/3}$ MeV, one would obtain a mass dependence proportional to $A^{-1/2}$ for the two-body matrix elements. The W interaction includes a mass dependence of the form $\langle V\rangle(A) = \langle V\rangle(A = 18)(A/18)^{-0.3}$, where the power -0.3 was imposed upon the least-squares fit. The $\langle V\rangle(A = 18)$ matrix elements of the W interaction are given in (22, 23). The introduction of this mass dependence for the W interaction was the key ingredient that made possible its improved accounting for sd-shell phenomena relative to that obtained in the immediately preceding work of Chung (10). Under the assumption of mass-independent two-body matrix elements, Chung & Wildenthal required two different sets of two-body matrix elements, one for the $A = 17$–28 region and one for the $A = 28$–39 region.

The $T = 0$ spectrum of ^{22}Na obtained with the W interaction as shown in Figure 2 is much improved compared to the results obtained with the renormalized G-matrix. Spectra for ^{27}Al, ^{28}Si, and ^{29}Si calculated with the W interaction are shown in comparison with experiment in Figure 3. For each nucleus the experimental excitation energies are plotted vertically on the right side, with lines joining them to the corresponding theoretical energies plotted on the left side. A horizontal line thus indicates perfect

agreement between experiment and theory. The slopes of the lines are typical of the 185-keV rms deviation obtained in the least-squares fit described above, although most of the levels shown here were not included in the iterative fit because of their large dimensions.

A complete examination of all sd-shell nuclei in comparison with excitation energies predicted with the W interaction shows that the quality of agreement shown in Figures 2 and 3 is typical for all $A = 21$–35 nuclei. (For $A = 18$–20 and 36–38, the sd-shell levels are fewer and the role of intruder configurations from the adjacent major shell is more important in the experimental spectra, thus lessening the quality of the overall correspondence between theory and experiment.) Beyond just this agreement in excitation energy for pairs of low-lying levels, further analysis (24) of recent experimental results (25–27) shows that the degrees of freedom of the sd-shell configurations, as guided by the W interaction, produce detailed agreement with experimental energies and spins for positive-parity levels on a one-to-one basis up through 6 or 7 MeV for nuclei from $A = 23$–33, where intruder effects are suppressed. The excitation energies of the lowest six to ten levels of each possible J value are correctly predicted, without either an excess or deficiency of levels, this agreement extending up to 10–15-MeV excitation energy for states with high J values.

Experimental and theoretical values of two-neutron separation energies of sd-shell ground states (values that are equivalent to ground-state binding energies in this context) are shown in Figure 4. The results obtained with the W interaction are shown as the thin solid lines, each indicating a chain of isotopes. The deviations between experiment and theory are indicated by the sizes of the circles at each N value. Most of the circles are quite small, well within the 185-keV rms overall deviation. A few large deviations occur for the most neutron-rich Na and Mg isotopes. These atypical deviations suggest the disappearance of the $N = 20$ shell closure for this region of the N-Z chart (see also 28, 29).

Extensive experimental studies are expanding our knowledge of the masses and excited-state energies of neutron-rich nuclei in the sd shell considerably beyond the situation indicated in Figure 4 (30-44). These studies further verify the predictions of the W interaction for these unusual N/Z ratios except, again, for the $A = 30$–32 Na and Mg isotopes. For these nuclei, the new data seem to confirm the earlier suspicion that sd-shell degrees of freedom do not describe the ground and low-lying excited states of these systems.

Spectroscopic factors obtained in single-nucleon transfer experiments provide simple and important tests of shell-model wave functions since they can be related to the integral and differential occupations of the individual single-particle orbits. The predictions of the W interaction for

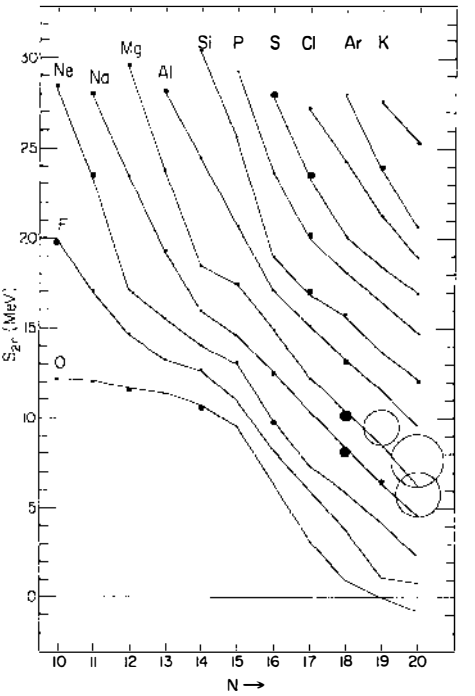

Figure 4 Two-neutron separation energies as a function of the neutron number N (see Section 2.1).

stripping and pickup on even-A sd-shell targets (B. H. Wildenthal, unpublished) agree with the consensus (45) of experimental results in every case, both for strong and weak-but-measurable states. The predictions for transfers from odd-A targets to even-A final nuclei (B. H. Wildenthal, unpublished) agree almost as well with experiment. The exceptions are several instances in which pairs of levels in doubly odd nuclei that have the same J value and are almost degenerate in energy have different predicted and observed relative strengths. Even in these cases, the sum of the observed strengths for each doublet is correctly predicted.

The depth and breadth of the agreement between experimental data for $A = 18$–38 states and the corresponding predictions of the W interaction for energies and spectroscopic factors strongly suggest that the physical states are dominated by 1s and 0d degrees of freedom and that the model wave functions incorporate these degrees of freedom in at least roughly the correct fashion. Thus it is appropriate to subject these wave functions to further scrutiny via comparisons with other types of experimental observables. The general class of experimental observables that are exam-

ined in Sections 3 and 4 correspond to one-body operators. Theoretically, the model wave functions are used to evaluate matrix elements of annihilation and creation operators for the single-nucleon orbits j coupled to specific ranks of isospin ΔT and angular momentum ΔJ. Different aspects of the wave functions are sampled as a function of the coefficients of the various components of the operators.

2.2 *Potential Models for Effective Shell-Model Interactions*

While the model-independent W interaction appears to be very successful for applications to sd-shell nuclei, its implications for shell-model studies in other mass regions, or for questions about the general nature of the effective interaction, are not transparent. Moreover, while the same model-independent approach can be used for heavier nuclei, the ratio of parameters to data worsens rapidly for the corresponding model spaces. Hence, the long-standing desire for procedures to link groups of two-body matrix elements together via a fundamental or an ad hoc relationship, or to eliminate some of them from the variation procedure altogether, remains a primary goal.

A fundamental technique in work with effective interactions is the transformation of the *jj*-coupled two-body matrix elements (TBME) into an LS-coupled representation (23, 46), in which the various components of the interaction (central, spin-orbit, tensor, and antisymmetric-spin-orbit) can be separated explicitly (23, 47). This is a unique transformation, and it makes no assumptions about the interaction other than the fundamental one that it is based on a two-body operator. If the effective interaction is derivable from an isospin-conserving potential that depends only on the relative and center-of-mass coordinates between two nucleons in the nucleus, then the antisymmetric spin-orbit (ALS) component must vanish. Several investigations of the ALS component have been carried out (23, 46, 48–51). For the W interaction it was found that the ALS component is not very important; setting this component to zero increased the rms deviation very little, from 185 to 215 keV (23).

Any attempt to limit the number of parameters defining the effective two-body interaction makes some assumptions, either implicit or explicit, concerning the parts of the interaction that are not varied. For example, some components could simply be set to zero, as just described for the ALS component. This treatment could also be applied to the spin-orbit and the tensor components, although with greater impact on the calculated results. In each case there would, of course, be a reduction in the number of free parameters remaining to vary in a fit to the data. As an alternative to setting these matrix elements to zero, they could, for example, be set equal to G-matrix values. Both of these possibilities have been explored

(23) in attempts to find the minimal number of parameters necessary to fit the experimental spectra.

As yet another approach to reducing the number of parameters necessary to specify the effective interaction, and as a means of providing a basis for extrapolating from the sd-shell to other mass regions, a potential, such as the one-boson-exchange potential (OBEP), can be defined for each component, with the various strengths and ranges adjusted to best fit the data. The strengths and ranges from such a fit can be compared to those obtained from fitting these same potential parameters to a *G*-matrix derived from nucleon-nucleon scattering potentials (52). Further elaborations can be added to the OBEP parameterization, such as density dependence and multipole-multipole terms. Each such elaboration would be motivated by the need to compensate for the effects of excluded configurations and the nuclear medium.

With such an approach, a 14-parameter, density-dependent OBEP has been determined that can reproduce the 447-element data set that determined the W interaction with an rms deviation of about 260 keV (23). The spectrum of ^{22}Na calculated with this interaction (SDPOTA) is shown in Figure 2. Applications of this potential model to the fp shell and other mass regions are under way (B. A. Brown, W. A. Richter, M. G. van der Merwe, R. E. Julies, unpublished).

It is interesting to compare the LS-coupled two-body matrix elements for the various sd-shell interactions discussed above. These matrix elements (23, 46) are shown in Figure 5 broken down into their central (C), spin-orbit (LS), tensor (T), and antisymmetric spin-orbit (ALS) components. It is interesting to see that all of these interactions appear to be qualitatively very similar. However, the relatively small differences between them are responsible for the dramatic differences in the quantitative description of the nuclear energy levels discussed above.

3. GAMOW-TELLER AND MAGNETIC DIPOLE MATRIX ELEMENTS

Measurements of magnetic moments, magnetic dipole (M1) gamma-decay transition rates, and Gamow-Teller (GT) beta-decay strengths provide relatively clear information about the structure of nuclear wave functions because the associated operators are simple and selective, coupling only a few single-nucleon orbits to each other. In addition, these operators do not couple to the first-order admixtures of "excluded" configurations into the "active" space, so that experimental values principally reflect the active space, corrected by second-order effects. In this section, comparisons of experimental values and predictions based on the W interaction are

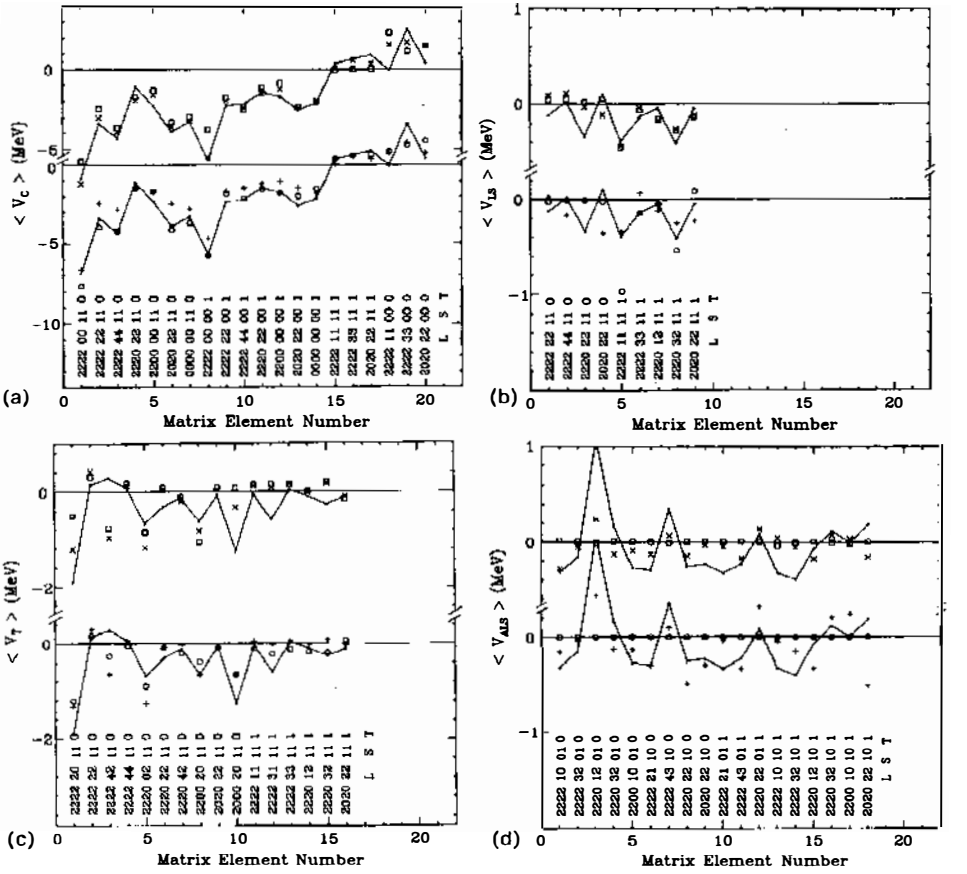

Figure 5 LS-coupled matrix elements for the central (*a*), spin-orbit (*b*), tensor (*c*), and antisymmctric spin-orbit (*d*) components of the sd-shell interactions. The upper and lower solid lines in each of the four panels connect points for the empirical W interaction discussed in Section 2.1. (The uncertainties associated with the W interaction are shown in the figures of Ref. 46). This is compared in the upper curve with the bare (*boxes*) and renormalized (*crosses*) G-matrix of Kuo (21). In the lower curve the W interaction is compared with the renormalized (SKSP4) *G*-matrix of Shurpin, Kuo & Strottman (19) (*pluses*) and with the empirical SDPOTA density-dependent OBEP interaction (*circles*) discussed in Section 2.2. The labels corresponding to the matrix element numbers along the x axis are the quantum numbers $l_a l_b l_c l_d$, LL′, SS′, and T in the LS-coupled matrix element $\langle l_a l_b$ LS $JT|V|l_c l_d$ L′S′ $JT\rangle$ where J is the maximum allowed by the vector coupling of L to S and L′ to S′.

reviewed with the dual goals of critiquing the model-space wave functions and characterizing the second-order corrections corresponding to excluded configurations.

Essentially the entire body of available M1 and GT data on sd-shell states has recently been compared with predictions of the W interaction (54–59). As examples here, we review results for cases in which the experimental data are accurate to 10% or better in the corresponding matrix elements. Comparisons between experiment and theory are presented in the form of scatter plots, in which the points correspond to a moment or a transition. The y coordinate of a plotted entry shows the experimentally determined value of the matrix element, and the x coordinate shows the corresponding theoretical value. Two different sets of theoretical values are shown for each set of observables, one obtained with the "free-nucleon" operator for the process in question (left panel) and the other based upon an "effective" operator (right panel). In these plots, agreement between experiment and theory thus corresponds to points lying on or about the 45° line.

3.1 *Free-Nucleon and Effective Operators*

The "free-nucleon" M1 and GT operators use, respectively, the electromagnetic and weak properties of free neutrons and protons as the coefficients of the spin, s, and orbital $\boldsymbol{l}$ angular momentum operators. Op(GT, free) $= |g_A/g_V|\mathbf{s}$ and Op(M1, free) $= g_s\,\mathbf{s}+g_l\,\boldsymbol{l}$, where $|g_A/g_V| = 1.251$ and g_s and g_l are the spin and orbital g factors for free nucleons. Combining these operator parameterizations with the wave functions of the active model space obviously leaves no provision for the effects of excluded configurations. The "effective" operators are formulated to allow for expression of such effects.

The effective M1 and GT operators for a single-particle wave function can be expressed in terms of corrections involving the three general types of rank-one operators $\mathbf{s}$, $\boldsymbol{l}$, and $\mathbf{p}$, where $\mathbf{p} = (8\pi)^{1/2}[Y^{(2)}\otimes\mathbf{s}]^{(1)}$. We express our results in terms of the δ parameters defined by the effective operator Op($\mathbf{x}$, effective) = Op($\mathbf{x}$, free)$+g_x[\delta_s(x)\mathbf{s}+\delta_l(x)\boldsymbol{l}+\delta_p(x)\mathbf{p}]$, where $g_x = |g_A/g_V|$ for x = GT and $g_x = g_s$ for x = M1. The M1 operator consists of both isoscalar (ISM1) and isovector (IVM1) parts, and the parameters associated with the ISM1 part can be expressed in terms of the spin expectation value parameters, δ(ISM1) = 0.423 δ(IS) (see 54, 58 for more details). In principle, one should introduce effective many-body operators for the many-body wave functions of A = 18–38, but empirical analysis indicates there is little need for them. Our single-particle correction operator does incorporate a mass dependence (54), $\delta(A) = \delta(A = 28)(A/28)^{0.35}$, which can be considered an effective two-body correction. Values for these

δ parameters can be empirically extracted as the residuals between a set of experimental values and the values of the matrix elements calculated with the free-nucleon operators. Our results are discussed in Sections 3.2 and 3.3 for the GT and M1 operators, respectively. Values for the δ parameters in the effective operator can also be calculated from fundamental considerations. Our empirical results are compared with such calculations in Section 3.4.

3.2 *Gamow-Teller Results*

The relationships between experimental GT matrix elements from sd-shell beta decays and the predictions of the W interaction have been studied comprehensively in (57). This study incorporated a compilation of extant beta decay in $A = 17$–39 nuclei together with shell-model calculations for all the initial and final states concerned. The essential conclusions drawn in (57) can be inferred from the comparisons of experimental and theoretical matrix elements presented in Figure 6. The values of the matrix elements are normalized to reflect the $3(N-Z)$ sum rule, such that $R(\mathrm{GT}) = M(\mathrm{GT})/W$, where $W = |g_A/g_V|[(2J_i+1)3(N_i-Z_i)]^{1/2}$ for $N_i \neq Z_i$ and $W = |g_A/g_V|[(2J_f+1)3(N_f-Z_f)]^{1/2}$ for $N_i = Z_i$. The matrix elements $M(\mathrm{GT})$ are obtained from $ft = 6170/[B(\mathrm{F})+B(\mathrm{GT})]$, where $B(\mathrm{GT}) = M(\mathrm{GT})^2/(2J_i+1)$. $B(\mathrm{GT})$ is the GT transition probability (which depends on the transition direction). $M(\mathrm{GT})$ is the GT reduced matrix element (which is independent of the transition direction).

It is evident from inspection of the left side of Figure 6 that the experimental values of GT matrix elements in the sd shell are systematically smaller than the predictions of the W-interaction wave functions coupled with the free-nucleon operator, by a factor of about 0.77 (indicated by the lower line on the left side of Figure 6). The same wave functions combined with the effective operator account for most of the data extremely well.

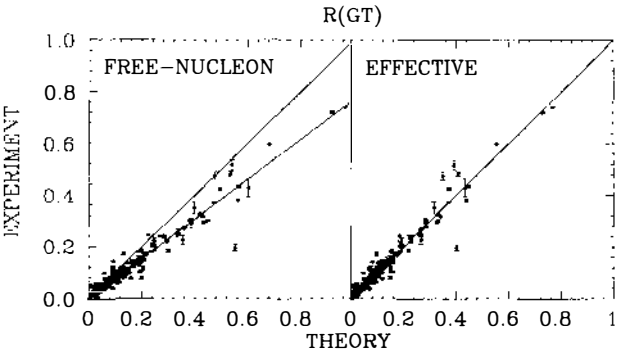

Figure 6 Theoretical vs experimental $R(\mathrm{GT})$ matrix elements (see Sections 3 and 3.2).

The essential feature of the correction is a quenching of the strength of the spin operator represented by a large, negative value of δ_s.

Some of the remaining deviations between experiment and theory can be attributed to incorrect predictions of the mixing of configurations between close-lying final states. This feature can be suppressed in the comparison by summing the strengths originating from a single initial state over several final states, as shown by the comparison of $T(\mathrm{GT})$ in Figure 7, where $T(\mathrm{GT}) = [\Sigma_f R(\mathrm{GT})^2]^{1/2}$. The size of $T(\mathrm{GT})$ is determined mainly by how much of the $3(N-Z)$ sum rule lies inside the beta-decay Q-value window. For two cases, $^{18}\mathrm{Ne} \rightarrow {}^{18}\mathrm{F}$ and $^{19}\mathrm{Ne} \rightarrow {}^{19}\mathrm{F}$, the sum rule is nearly exhausted by a single final state, while in others only a very small fraction is found.

These results, obtained from standard beta-decay data on mostly near-stable nuclei, suggest a major and systematic effect. The possible universality of this effect can be studied by expanding the scope of comparisons to new regions of nuclei, new Z/N ratios, and larger ranges of excitation energy. Within the sd shell, considerable work is being done along these lines by measuring far-from-stable nuclei and studying higher ranges of excitation energy through measurements of beta decays from very proton-rich nuclei. Larger spans of excitation energy are also being studied through use of hadronic analogues of beta decay such as the (p,n), (n,p), and (p,p′) reactions. Extensions of such studies to regions outside the sd shell are hindered, except for the p shell (60), by the difficulties of calculating in a full oscillator shell. Truncations that limit conversions between spin-orbit partners have large effects upon predicted matrix element magnitudes (61).

The ongoing studies of very neutron-rich sd-shell systems (37, 60, 62–67) confirm the general efficacy of the W-interaction wave functions and

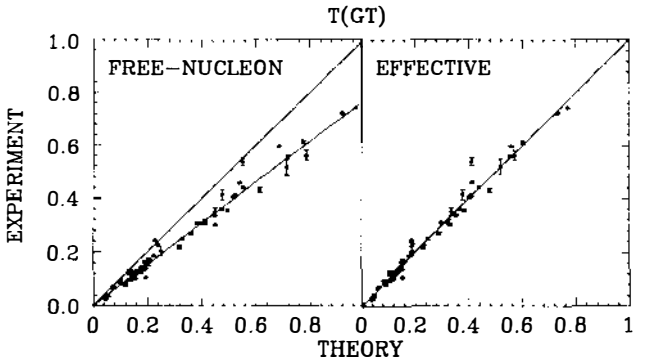

Figure 7 Theoretical vs experimental $T(\mathrm{GT})$ matrix elements (see Sections 3 and 3.2).

the effective, quenched, GT operator, except for the region of nuclei localized around ^{31}Na and ^{32}Mg, where, as noted, the analysis of energies already suggested the disappearance of the $N = 20$ shell closure. New results from the ISOLDE, NSCL, and GANIL facilities will provide important additional tests of these ideas, especially as detailed decay studies elucidate the levels and spins of these exotic nuclei.

Since the GT strength is typically centered around an excitation energy corresponding to the spin-orbit splitting, a definitive study of this phenomenon requires examination of regions of excitation energy much higher than are accessible from conventional beta-decay processes. This restriction can be partially circumvented by studying the decay of very proton-rich nuclei that have large Q values (68–71). More generally, the exploitation of the (p,n) and (p,p′) reactions, which at medium bombarding energies and at 0° detection angle are closely analogous to the GT operator, have provided extremely illuminating information on nuclear wave functions and GT strength by eliminating the Q-value constraint completely. Such studies (72–82) confirm that the sd-shell wave functions generated with the W interactions distribute GT strength correctly up through about 20 MeV of excitation energy and that the quenching of the effective GT operator inferred from low-excitation-energy data remains constant up to high excitation energies.

The ^{26}Mg(p,n) experiment provides an example of the information that can be obtained from analysis of hadronic "GT" data. The distribution of "GT" strength extracted from the reaction data (78) is compared with the distribution calculated from the W wave functions in Figure 8. Both theory and experiment have been Gaussian averaged over 2 MeV in order to emphasize the gross structure. Only the peak around 1 MeV in excitation

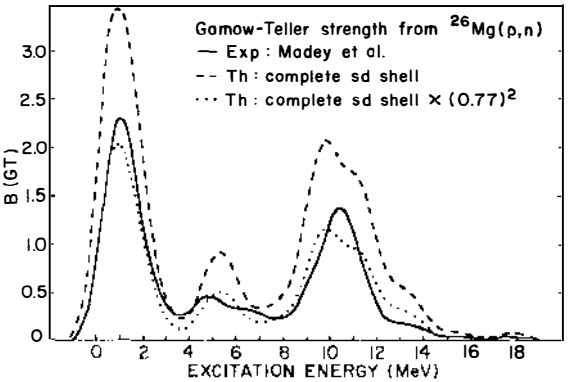

Figure 8 Theoretical vs experimental Gamow-Teller strength functions for ^{26}Mg→^{26}Al (see Section 3.2).

lies within the Q-value window of the GT beta decay to ^{26}Al from the analogue "target" ^{26}Si. The calculated distribution with the free-nucleon GT strength is larger than experiment at all excitation energies. This same distribution function is in good qualitative agreement with experiment when it is multiplied by $(0.77)^2 = 0.6$. The "missing" GT strength is not to be found, at least up to an excitation energy of about 20 MeV, for the sd-shell nuclei.

This reduction factor of 0.6 is consistent with the analysis of GT and (p,n) data in the fp shell (61, 83–85). The GT strength extracted from (p,n) experiments on nuclei up to the Pb region is systematically "quenched" relative to $3(N\text{-}Z)$ by about this same factor (86). New (n,p) experiments such as those being performed at TRIUMF (87, 88) will provide valuable information on the final-state isospin dependence of the GT strength. As an approximation for heavier nuclei, an occupation-number-dependent GT sum rule was proposed by MacFarlane (219). We note that this approximation is very poor for the sd shell (220).

3.3 *Magnetic Dipole Results*

The M1 electromagnetic excitation and decay of sd-shell states should correspond closely to GT beta decay. The M1 operator incorporates both the spin orbital operators and acts in both the isovector and isoscalar channels, but the coefficient of s is much larger than that of l and that of the isovector channel much larger than that of the isoscalar. Hence, there should be a strong resemblance between the gross features of M1 decay and those of the isovector (s) GT operator, while the detailed differences between them should also be informative. Experimental M1 matrix elements derived from gamma-decay transition data (B. H. Wildenthal, J. Keinonen, unpublished) are compared with predictions of the W interaction in Figure 9. The matrix elements are defined such that

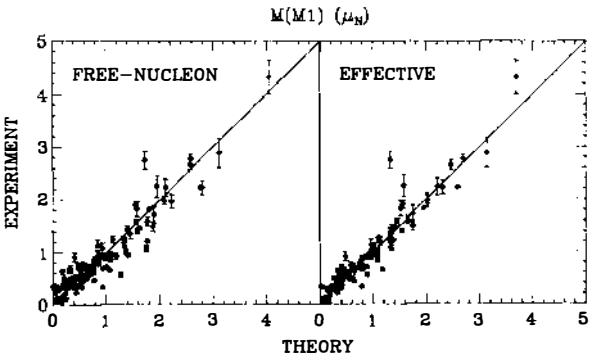

Figure 9 Theoretical vs experimental M1 γ-decay matrix elements (see Sections 3 and 3.3).

$B(\mathrm{M1}) = M(\mathrm{M1})^2/(2J_i+1)$. The free-nucleon predictions in the left panel do not appear to require any overall adjustment in order to improve agreement with experiment, in contrast to the case for GT beta decay. However, the scatter of points about the 45° line is reduced significantly when the W wave functions are combined instead with the effective operator. Hence, there is little net quenching from the empirical corrections to the M1 operator; however, in a more complicated interference between the spin and orbital contributions, the corrections serve to reduce some theoretical matrix elements and increase others, generally in the directions of the experimental values.

Likewise, the M1 matrix elements deduced from experimental values of magnetic moments (89) are reproduced quite well with the free-nucleon version of the predictions, and the effective operator produces even closer agreement, as can be seen in the left and right panels of Figure 10, respectively. Since, as we noted, both the GT and the M1 operators are dominated by the isovector spin term, it is surprising to find that the free-nucleon predictions for the M1 matrix elements are in much closer agreement with experiment than are the free-nucleon GT predictions.

To pursue the issue further, we note that the isovector and isoscalar components of the Ml operator can be isolated by constructing the difference and sum, respectively, of the matrix elements for mirror moments and transitions (54). The isovector matrix elements of sd-shell moments are shown in Figure 11, and the isoscalar moments are shown in Figure 12. In addition to the moments treated in (54), Figures 11 and 12 include the results from the recent measurement of the ^{33}Cl magnetic moment (90). (We note that only the magnetic moments of the ground states of ^{23}Mg and ^{37}Ar remain to be accurately measured in order to complete the experimental data for sd-shell mirror moments.) In Figure 12, the isoscalar

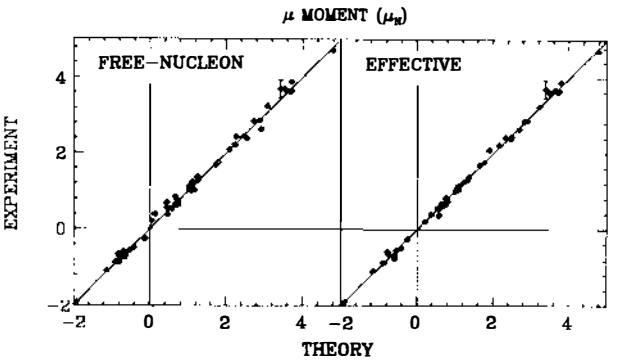

Figure 10 Theoretical vs experimental magnetic moments (see Sections 3 and 3.3).

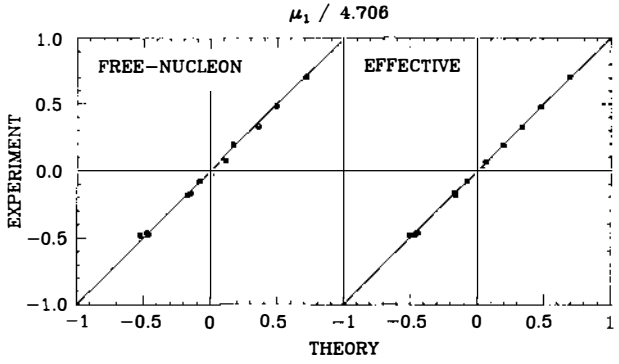

Figure 11 Theoretical vs experimental isovector M1 matrix elements (see Sections 3 and 3.3).

moments have been converted into the equivalent spin matrix elements, as in (54).

The relationship between the two isovector theories and experiment shown in Figure 11 is as expected from Figure 10, given the dominance of the isovector component of the total M1 operator. However, the relationship between the free-nucleon predictions of the isoscalar moments and experiment indicates the need for a significant correction to the free-nucleon operator. The deviations cannot be explained simply in terms of an overall reduction factor. This would correspond to the rotated dashed line in the left panel of Figure 12. Rather, both the spin and the orbital components of the isoscalar operator require corrections. The effective

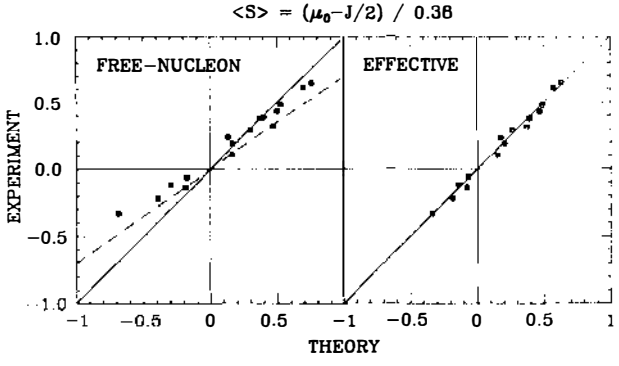

Figure 12 Theoretical vs experimental isoscalar M1 matrix elements (see Sections 3 and 3.3).

operator derived from isoscalar moments is consistent with the quenching found for isoscalar M1 transitions (59, 79).

These M1 moment and decay studies can be extended to higher excitation energy with photon and electron bombardments of stable ground states. Such studies can test the consistency of the shell-model accounting over extended regions of excitation energy (91, 92). Since the configurations dominating the wave functions change, on the average, with excitation energy, these energy-dependent comparisons are an important adjunct to the mass-dependent comparisons that conventional data provide. In heavier nuclei, experimental M1 matrix elements are usually compared with predictions based on model wave functions that do not yet include configuration mixing between the spin-orbit partners. (This type of configuration mixing is included to all orders in our sd-shell wave functions.) In this case the difference between experiment and theory is usually dominated by the "first-order" configuration-mixing correction (e.g. 93, 94).

3.4 *Empirical versus Theoretical Corrections for Excluded Configurations*

Extensive theoretical studies have been made of the corrections to the GT and M1 operators for sd-shell systems that are needed to compensate for excluded configurations and neglected nucleonic and mesonic degrees of freedom. Reviews of these studies by Towner (94) and Arima et al (95) have recently appeared. In Figure 13 we compare our empirical values for the δ parameters discussed in Section 3.1 extracted from the comparisons discussed in Sections 3.2 and 3.3 with the theoretical results obtained by Arima et al (ASBH) and Towner & Khanna (TK) (96). (We note that updated and somewhat modified results are given in Towner's review and we refer the reader to this review for a comparison of these with our empirical results.) The empirical values derived from the fits to the $A = 17$–39 mass region are scaled to $A = 39$ by the assumed mass dependence $\delta(A) = \delta(A = 28)(A/28)^{0.35}$ and are compared to the calculations based on one hole in a ^{40}Ca closed-shell configuration. The error bars on the empirical results reflect the rms deviation in the fit of the effective operator predictions to experiment, together with the errors in the experimental data. Three separate components of the theoretical corrections are shown in addition to the net results, those arising from (*a*) high-order configuration mixing (CM), (*b*) mesonic exchange currents involving the Δ isobar, and (*c*) other mesonic-exchange currents (MEC), such as the one-pion-exchange and the pionic pair diagrams. It is important here to remember that the first-order configuration mixing that dominates the corrections for excluded configurations for operators such as E2 (see

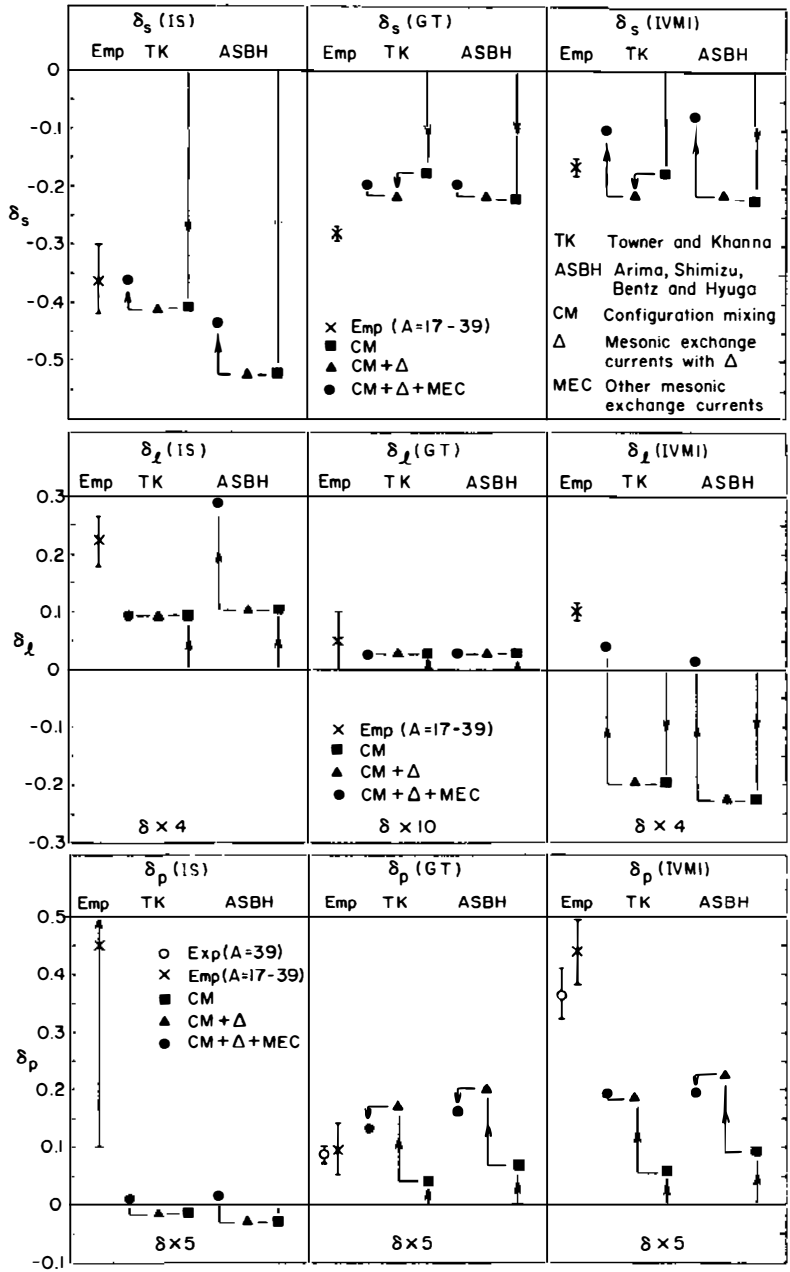

Section 4) are not present for the simple, radial-independent M1 and GT operators.

A number of interesting conclusions can be drawn from these comparisons. The empirical value of δ_s(IS) derived from isoscalar moments is quite large and is in good agreement with both calculations. The calculated quenching comes mostly from configuration mixing with a little enhancement from MEC. The first-order Δ isobar contributions vanish in this case because the particle-hole vertex must change isospin by one unit.

The empirical value of δ_s(GT) is about 50% larger in magnitude than the calculated values. Again, the calculated quenching comes mostly from CM. For both δ_s(IS) and δ_s(GT) the CM contribution is dominated by the tensor interaction, and the ratio $\delta_s(\mathrm{GT,CM})/\delta_s(\mathrm{IS,CM}) \approx 0.42$ is very insensitive to details of the CM calculation (95). Thus, with CM alone it is difficult to explain the additional empirical GT quenching without destroying the agreement for the isoscalar moments.

The importance of the Δ contribution to δ_s(GT), however, remains controversial. For example, Oset & Rho (97) obtain $\delta_s(\mathrm{GT},\Delta) = -0.15$, as compared to -0.038 from Towner & Khanna and to 0.004 from Arima et al. Such differences arise from the assumptions made about short-range correlations, exchange terms, and crossing terms. Agreement with our empirical value would be obtained with $\delta_s(\mathrm{GT}) \approx -0.10$, a value intermediate to the extremes of the predictions. We note that the agreement to $\delta_s = -0.10$ can be improved within the model of Oset & Rho by using a more recent estimate of the Landau parameter g'_Δ (98). From the above consideration, we conclude that the amplitude of the "quenching" observed for the Gamow-Teller operator is derived approximately two thirds from higher-order configuration mixing and one third from Δ admixtures.

The predicted values of δ_s for the GT and the isovector M1 (IVM1) operators differ only in the MEC component. The CM and Δ corrections each contribute equally to GT and IVM1 because the corrections are dominated by the (nonrelativistic) $\sigma\tau$ operator in both cases. On the other hand, the MEC contribution depends upon the underlying relativistic structure, i.e. axial-vector for GT and vector for M1. It turns out that the MEC corrections for the GT operator, which arise mainly from the ρ-π diagram, are small relative to the one-pion-exchange contribution for the M1 operator. The empirical difference $\delta_s(\mathrm{IVM1}) - \delta_s(\mathrm{GT}) \approx 0.12$ is in fair agreement with the MEC calculations.

Figure 13 Empirical δ parameters (scaled to $A = 39$) compared with two calculations (see Section 3.4).

The empirical values of δ_l are in fair agreement with the predictions. The early versions of the relativistic σ-ω model (99) appeared to give extremely large corrections to the M1 orbital operator, as a consequence of the M^*/M factor (100). In fact, this was one of the early reasons for rejecting such models. For the isoscalar moments it now appears that there are nuclear-medium corrections, "backflow" diagrams, which essentially bring the result closer to the standard (nonrelativistic) model, at least for the isoscalar term (101–105).

The empirical value for δ_l(IS) is about twice as large as the calculated CM contribution. The Arima et al predictions incorporating the new calculations for the MEC somewhat overshoot the empirical value. For δ_l(IVM1) the agreement between experiment and theory seems good in the light of the very large cancellation between the CM and MEC contributions. There still seems to be room for some "relativistic" corrections (105) for the IVM1 orbital g factor.

The δ_p comparison in Figure 13 includes values derived from the "single-particle" $3/2^+ \rightarrow 1/2^+$ transitions in $A = 39$ (106), which are consistent with those obtained in our global ($A = 17$–39) analysis. The large error in the empirical δ_p(IS) value precludes any meaningful comparison with the small theoretical corrections. The calculated δ_p corrections for GT and IVM1 are similar in value and dominated by the Δ isobar correction. The agreement for GT is good, but the empirical correction for the isovector M1 transitions is nearly twice as large as that calculated. At present this discrepancy is not understood.

4. ELECTRIC QUADRUPOLE MATRIX ELEMENTS

Experimental E2 matrix elements derived from gamma-decay transition data (B. H. Wildenthal, J. Keinonen, unpublished) are compared with predictions of the W interaction in Figure 14. The matrix elements are defined by $B(\mathrm{E2}) = M(\mathrm{E2})^2/(2J_i+1)$. A similar comparison (107) for electric quadrupole moment data (89, 108–111) is shown in Figure 15. The E2 matrix elements are more complicated than those for the M1 and GT operators because they require specification of the radial wave functions. We have considered many parameterizations for the radial wave functions (107, 112, 113). For simplicity here we use the harmonic oscillator form with $\hbar\omega = 45A^{-1/3} - 25A^{-2/3}$.

The left panels of Figures 14 and 15 show comparisons with predictions based on the use of free-nucleon charges, $e_p = 1e$ and $e_n = 0$, in the E2 operator. As is evident, the experimental values are uniformly larger than these predictions. The scale factor is about 1.8, as indicated by the dashed line in Figure 14 and the line with an increased slope in Figure 15. A two-

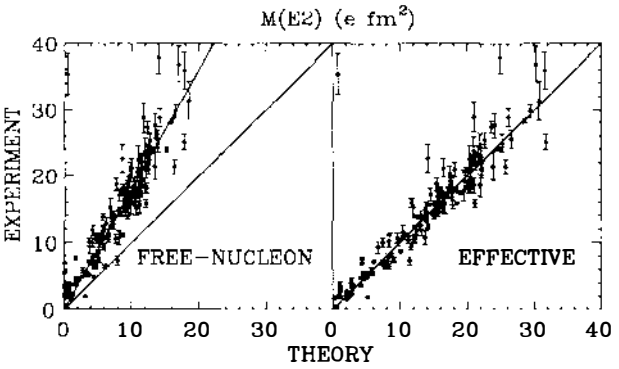

Figure 14 Theoretical vs experimental E2 gamma-decay matrix elements (see Section 4).

parameter least-squares fit of the shell-model densities to these E2 data yields values of $e_p+\delta e_p+\delta e_n = 1.78(3)e$ for the isoscalar "effective" nucleon charges and $e_p+\delta e_p-\delta e_n = 0.8(1)e$ for the isovector. These values have been used to generate the effective operator predictions shown in the right panels of the figures. With a few exceptions, the agreement between experiment and effective operator predictions is excellent.

The E2 matrix elements between low-lying states are dominated by the isoscalar component of the operator; for this reason, the effective isoscalar charge is well determined from a comparison between experimental values and the shell-model predictions coupled with the free-nucleon charges. The effective isovector charge is poorly determined because the isovector

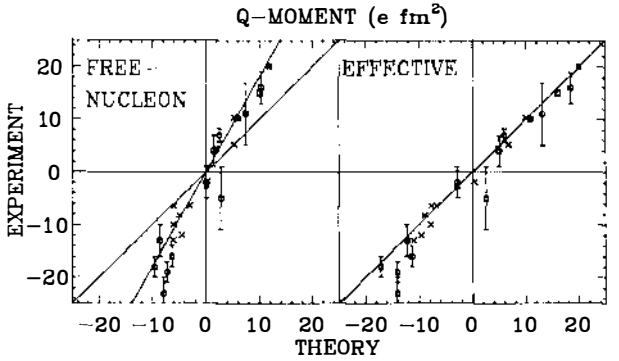

Figure 15 Theoretical vs experimental quadrupole moments (see Section 5). These data include the atomic measurements (89) (*crosses*), as well as more recent data for the 2^+ states from Coulomb excitation experiments (108) (*circles with error bars*) and from muonic atoms (109, 110) (*squares with error bars*). Error bars are not given for the atomic data because of the unknown uncertainties associated with the Sternheimer corrections (111).

component of the total E2 matrix element typically is small relative to the experimental errors and to the deviation between the theoretical and experimental values of the total matrix element. The isovector term can be isolated by looking at the differences between transitions in mirror nuclei (113). In this analysis the effective isovector charge was determined to be quite sensitive to the radial component of the single-particle wave functions, because many of the strong isovector transitions occur between loosely bound states in the lower part of the shell. The results ranged from $e_p+\delta e_p-\delta e_n \approx 1.0e$ with harmonic oscillator radial wave functions to $e_p+\delta e_p-\delta e_n \approx 0.65e$ with the more realistic Woods-Saxon radial wave functions. The use of the Woods-Saxon wave functions reduces the isoscalar effective charge in these analyses to about $1.60e$.

The study of isovector E2 matrix elements can be directed toward the issue of whether specific shell-model wave functions correctly predict the sign and magnitude of this term, relative to the isoscalar term. This topic has been pursued with gamma-ray decay lifetime measurements (114–116), with measurements of the ratios of π^-/π^+ inelastic scattering strengths (117), and with comparisons between other hadronic probes (118–123). The hadronic probes depend upon both the proton and neutron components of the wave functions (124, 125). The agreement of experiment with the calculated sd-shell matrix elements for the lowest two 2^+ states is good, with the exception of the second 2^+ $T=1$ multiplet in $A=34$ (114, 125, 126).

It is well known that the first-order coupling of the valence states with the $2\hbar\omega$ giant quadrupole states is the primary source for the charge renormalization (e.g. 112, 127). One of the most recent calculations was based on the SGII Skyrme-type interaction (128) and gave average values of $e_p+\delta e_p+\delta e_n = 1.68e$ and $e_p+\delta e_p-\delta e_n \approx 0.78e$, in good agreement with the ranges for the empirical values quoted above.

5. HIGHER-MULTIPOLE MATRIX ELEMENTS AND ELECTRON SCATTERING FORM FACTORS

Elastic and inelastic electron scattering measurements can extend the information available from M1 and E2 moment and gamma-decay data. They yield additional multipolarities and a range of momentum-transfer values. For the sd shell, the phenomena comprise the C0, C2, and C4 longitudinal form factors and the M1, E2, M3, E4, and M5 transverse form factors (129). The elastic C0 data (and related rms radii data) are used primarily to parameterize the phenomenological radial potentials (130). Inelastic C0 transitions appear to be dominated by non-sd-shell components (131).

The inelastic longitudinal (e,e′) spectra for the sd-shell nuclei are dominated by the C2 and C4 multipoles. The experimental C2 form factors typically are a factor of three larger at the first maximum than those calculated with the free-nucleon charges. However, the experimental C2 values can be accurately predicted over a range of momentum transfers up to at least 2.5 fm^{-1} by combining the free-nucleon contribution from the valence orbits with a contribution from excluded configurations. One model for this latter contribution is a Tassie model form factor normalized to reproduce the E2 effective-charge parameters δe_p and δe_n discussed in Section 4 (130).

The experimental C4 form factors are typically a factor of four larger than the free-nucleon calculations. Quantitative agreement in nearly all cases can be obtained by adding a similar correction for excluded configurations, in this case normalized to effective charge values of $e_p+\delta e_p+\delta e_n = 2.0e$ and $e_p+\delta e_p-\delta e_n = 1.0e$ (130, 132). The level of agreement that can be obtained for the shapes and magnitudes of relatively strong C2 and C4 form factors is illustrated in Figure 16 with the example of ^{32}S(e,e′) transitions to the second 2^+ and first 4^+ states (132). The individual multipoles are indicated by the crosses (C2) and the dashed line (C4). The predicted form factor for this doublet is dominated by the C4 term and is in excellent agreement with experiment.

It may seem surprising that the effective C4 isoscalar charge (2.0e) is

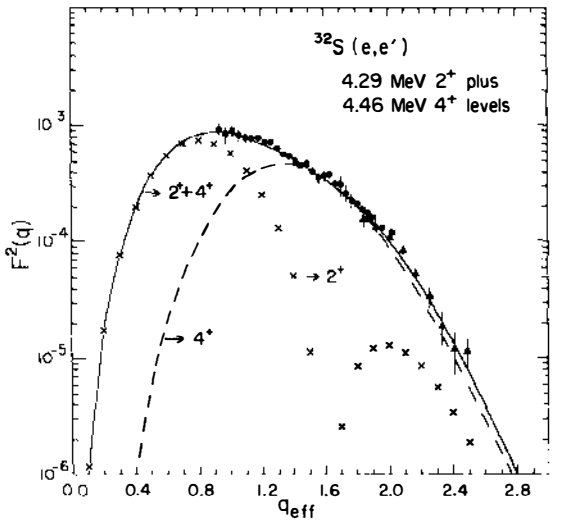

Figure 16 Longitudinal (e, e′) form factor for the unresolved 4.29–4.46-MeV doublet in ^{32}S (see Section 5).

larger than the effective C2 isoscalar charge (1.6–1.8e). However, this larger value is consistent with a calculation for the coupling of the sd-shell valence orbits to the C4 giant resonance (126). It would be interesting to continue such comparisons for the higher-multipole ($L > 4$) longitudinal form factors in heavier nuclei.

Given these state-independent and mass-independent effective-charge ingredients, the predicted C2 and C4 strength distributions are usually in excellent agreement with experiment up to excitation energies of about 6–8 MeV. As an illustration of this excitation-energy aspect, Figure 17 shows a comparison of the calculated (133; R. Radhi, B. A. Brown, B. H. Wildenthal, unpublished) and measured (134) ^{27}Al (e,e′) spectra at 90° and $E_e = 177$ MeV ($q \approx 1.3\,\mathrm{fm}^{-1}$). At this angle the spectrum is dominated by the longitudinal C2 and C4 terms. The states in the experimental spectrum labeled with arrows are known to be positive-parity states. The theoretical spectrum has been plotted with a resolution to match that of the experiment.

Transverse M1 form factors provide an important extension of the M1 moment and gamma-decay data discussed in Section 3.3. Such data have been obtained from the transverse elastic scattering from the stable $1/2^+$

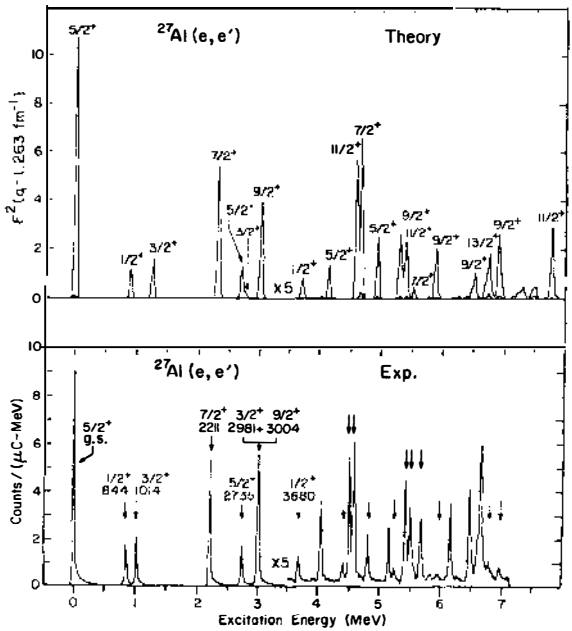

Figure 17 Theoretical (*top*) vs experimental (*bottom*) spectrum for ^{27}Al(e,e′) at 90° and $E_e = 177$ MeV (see Section 5).

ground states of ^{19}F (135), ^{29}Si and ^{31}P (136). The ^{19}F data are compared in Figure 18 to the predictions of the W interaction combined with the free-nucleon operator. These calculations (129, 137), indicated by the solid lines of the figure, used harmonic oscillator radial wave functions with $b_{rms} = 1.83$ fm, a value chosen to fit the measured rms charge radius.

As always, it is important to consider corrections for excluded shell-model configurations and omitted particle currents. The left panel of Figure 18 shows some corrections (P. G. Blunden, private communication, 1986) based on the formulation of Blunden & Castel (139). The crosses include the effect of first-order (1p-1h) configuration mixing (FCM) (which goes to zero at $q = 0$), the dash-dot line includes the effects of FCM plus higher-order configuration mixing (FCM+CM), and finally the dashed line includes the effect of FCM plus CM plus mesonic exchange currents (FCM+CM+Δ+MEC). The dashed line is compared with experiment on the right side. It is apparent that the FCM correction dominates and that this correction alone is enough to explain qualitatively the double minimum suggested by the data.

Similar comparisons are made in Figure 19 for the ^{20}Ne inelastic M1 form factor for the transition to the $T = 1$ $J^{\pi} = 1^{+}$ state at 11.26 MeV. The data are from Darmstadt (*crosses*) and Mainz (*circles*) (J. C. Bergstrom, private communication, 1983). The predictions use harmonic oscillator wave functions with $b_{rms} = 1.87$ fm. In this case the MEC corrections are

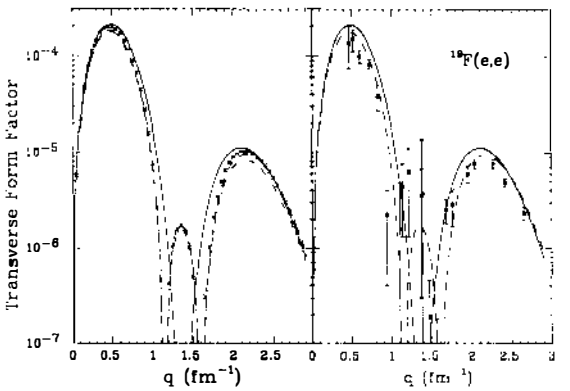

Figure 18 Transverse elastic form factor for ^{19}F (see Section 5). The solid line shown in both panels is the free-nucleon prediction. The dashed line shown in both panels is the prediction that includes corrections for first-order configuration mixing (FCM), higher order configuration mixing (CM), and mesonic-exchange currents, including those involving the Δ isobar. In the right panel, these two predictions are compared with experiment (135). In the left panel, effects of the individual corrections are shown; the crosses include FCM and the dash-dot line includes FCM plus CM.

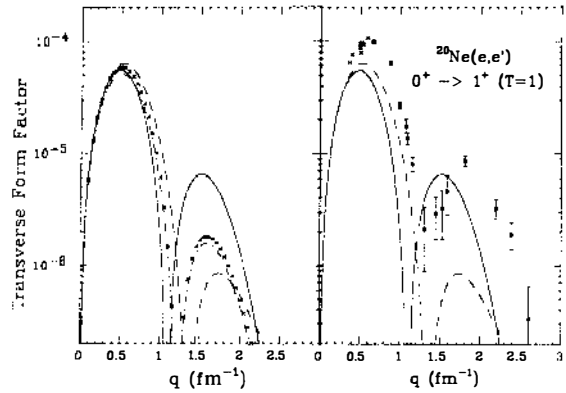

Figure 19 Transverse inelastic form factor for the 11.26-MeV 1^+ $T = 1$ state in ^{20}Ne (see Section 5). The symbols are explained in the caption to Figure 18. The experimental data are from J. C. Bergstrom (private communication, 1983).

relatively more important. While the corrections for excluded configurations improve the agreement of theory with experiment, there is still a serious disagreement in this case. Clearly, something is missing in the calculation. The W interaction predicts that this state has a large orbital component at small q (141–144), and this has been confirmed in a recent (p,p′) experiment (142).

The elastic transverse form factor for ^{27}Al, shown in Figure 20, is

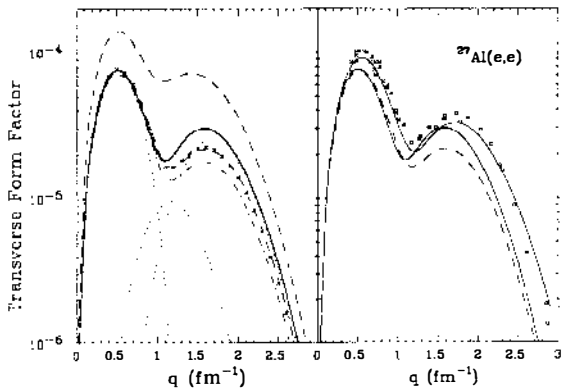

Figure 20 Transverse elastic form factor for ^{27}Al (see Section 5). The symbols are explained in the caption to Figure 18. In addition, in the left panel the individual multipole contributions (M1, M3, and M5) are shown by the dotted lines, and the pure $d_{5/2}$ single-particle prediction is shown by the upper dashed line. Also, in the right panel the free-nucleon prediction obtained with a harmonic oscillator length parameter reduced by 10% from the value used in the standard calculation is shown by the upper solid line. The experimental data are from (145).

an example involving all three magnetic terms, M1, M3, and M5. (The individual contributions are shown by the dotted lines on the left.) The data are taken from the review of Donnelly & Sick (145). The calculations are as described above, using harmonic oscillator wave functions with $b_{rms} = 1.80$ fm. The upper dashed line in the left panel is the form factor predicted for the pure single-particle $d_{5/2}$ configuration. For ^{27}Al the addition to the free-nucleon calculations of the predicted corrections for excluded configurations and currents lessens the agreement of theory with experiment. It is interesting to note that this agreement can be made nearly perfect if we simply modify the free-nucleon sd-shell calculation by reducing the oscillator length by 10% (the upper solid line in the right panel). This change, while not large, is nonetheless difficult to justify. It is reminiscent of similar simple cures to the notorious Nolen-Schiffer anomaly regarding Coulomb displacement energies of analogue states (146).

These last few examples are typical of current problems in understanding transverse form factors. Data on the pure E2, M3, E4, and M5 multipolarities, which can be obtained from the transverse electron scattering from $J = 0^+$ targets such as the M3 discussed by MacGregor et al (147) or the E4 we proposed (148), are especially valuable.

6. STUDIES IN OTHER MASS REGIONS

In this section we discuss briefly recent shell-model research (since about 1980) that deals with mass regions other than $A = 17$–39. Some earlier work is reviewed by McGrory & Wildenthal (9). We limit the present discussion principally to studies that are close in spirit to the "large-basis" type of shell-model calculations discussed above for the sd shell. The only completely analogous study is, as mentioned, the precursor study of $A = 6$–15 nuclei with the complete space built from the $0p_{3/2}$ and $0p_{1/2}$ active orbits (14). Studies of nuclei in the $20 < N,Z < 40$ region with fp-shell configurations provide the next closest approximations to the sd-shell studies. However, this model space is less than ideal at the upper end of this mass range because it omits the $0g_{9/2}$ orbit, which is an integral component of low-lying excitations for the heavier systems. Moreover, the dimensions of the states incorporating the full set of basis vectors from the four-orbit space increase very rapidly to very large numbers with increasing numbers of active particles.

As a consequence of these dimension issues, calculations in the complete fp-shell space are currently possible only up to about $A = 45$ for low values of the isospin and for the Ca isotopes (149–151). Beyond this, most calculations are restricted to truncations that are equivalent (with respect

to a closed $0f_{7/2}$ shell for ^{56}Ni) to the excitation-first-order approximation for ^{28}Si discussed in Section 2. Effective interactions for the excitation-first-order fp model space have been developed by van Hees & Glaudemans (152), Mooy & Glaudemans (153), and Yokoyama & Horie (154). Particle-transfer, electromagnetic, and GT observables in this first-order model space have been studied with the van Hees & Glaudemans interaction (61, 85, 152), the Mooy & Glaudemans interaction (153, 155), and the Yokoyama & Horie interaction (154, 156–158), as well as with earlier versions of these approaches (159–163). Other recent studies in the fp shell include (84) and (164).

Beyond the fp shell, "full-space" calculations are limited to the systems of identical nucleons (all protons or all neutrons) relative to a pair of doubly closed shells or to proton-neutron systems very close to such a doubly closed shell. For the $N = 50$ isotones with $Z = 29$–50, calculations by Ji & Wildenthal (165) have encompassed the most complete basis yet studied, comprised of the $0f_{5/2}$, $1p_{3/2}$, $1p_{1/2}$, and $0g_{9/2}$ proton orbits and incorporating some internal truncations. For nuclei around $A = 90$ ($N = 48$–50 and $Z = 38$–50) the smaller $0g_{9/2} - 1p_{1/2}$ model space continues to be useful (166–170), although there are many known excited states that require additional configurations (165, 171–173).

Recent studies of still heavier nuclei are also available. Calculations for the Sn isotopes have been reported by Momoki et al (174) and Prade et al (175). The $N = 82$ isotones have been considered with a model space based on the $0g_{7/2}$, $1d_{5/2}$, $1d_{3/2}$, $2s_{1/2}$, and $0h_{11/2}$ proton orbits (176–178). Properties at the higher end ($Z > 62$) of this $N = 82$ model space are dominated by the simple spectra associated with an isolated $0h_{11/2}$ orbit (179–183). There is also recent work in the Pb region (184–188).

For the very light nuclei ($A = 3$–20) it is now possible to consider model spaces in which many major oscillator shells are active. In these cases "model-independent" interactions are completely impractical because of the very large number of two-body matrix elements involved. As an alternative, such calculations usually are based on some reasonable microscopic or heuristic two-body potential model for the interaction. Another new problem that must be addressed in such many-major-shell calculations is the elimination of the spurious components of the space that arise when the space extends beyond "$0\hbar\omega$" and that correspond to center-of-mass excitation. This elimination is fairly straightforward as long as the basis is complete (189, 190).

Two recent examples of such studies for very light nuclei are calculations for ^{4}He within a full $10\hbar\omega$ basis (191) and for $A = 6$ within a full $6\hbar\omega$ basis (192). Excited states in nuclei up to about $A = 20$ have been studied in a full $1\hbar\omega$ (s-p-sd) model space. The original Millener-Karath interaction

(193) and modified versions of it continue to be used with success in this $1\hbar\omega$ model space (60, 194–202). Van Hees & Glaudemans (203) have more recently developed a new interaction based on a comprehensive study of both $0\hbar\omega$ and $1\hbar\omega$ excitations for many nuclei in the $A = 4$–16 mass region. This work has recently been extended to include magnetic moments in the determination of the effective interaction (204). Similar work is being started for the sd-pf model space for nuclei in the $A = 35$–39 region (205–209).

It is technically feasible to calculate the spectra of nuclei up to about $A = 18$ in a complete $2\hbar\omega$ (s-p-sd-fp) model space. Such calculations for ^{16}O are straightforward (210), and calculations over the entire $A = 4$–16 mass region with an adjusted interaction have recently been reported (211). However, these configurations tend to mix strongly with the $0\hbar\omega$ states, and there is a severe problem of the excitation-order convergence (210) analogous to the problem for ^{28}Si within the sd shell discussed in Section 2. Also, in this case one must consider the Hartree-Fock condition concerning the mixture of the $2\hbar\omega$ 1p-1h component into the closed-shell ground state. A complementary understanding of these cross-shell excitations can be obtained from complete calculations within a small subspace such as $p_{1/2}$-$d_{5/2}$-$s_{1/2}$ for the $A = 16$ region (212) and $d_{3/2}$-$f_{7/2}$ for the $A = 40$ region (213; see also 214). Calculations of the spectrum of ^{16}O within a complete $4\hbar\omega$ model space should be possible in the near future.

7. PROSPECTS FOR THE FUTURE

The success of the comparisons presented above illustrates the efficacy of the modern multiconfiguration shell-model approach to understanding nuclear phenomena. There may still be room for improvement in the sd-shell calculations, but it is not clear from what direction it will come. Perhaps some further adjustments of the two-body matrix elements will help. Feedback from the properties of exotic nuclei as well as the electromagnetic and beta-decay data should help to tie down some of the poorly determined two-body matrix elements. For other data, such as C0 form factors and some of the transverse magnetic form factors, it appears that non-sd-shell contributions must be included at a more explicit level than as effective operators, in ways that are as yet not understood.

The sd-shell results should provide a touchstone for other extended shell-model calculations. The fp shell is the next logical challenge. Although much progress has been made in the fp shell, away from the $A = 48$ and $A = 56$ $f_{7/2}$ closed shells most calculations are still carried out at the level equivalent to excitation-order-one in Figure 1, with only a few at the level of excitation-order-two. At the upper reaches of the fp shell

the situation is further complicated by the presence of the "intruder" high-spin orbitals from the next higher major shell. Cross-shell excitations in light nuclei, and in particular the mixing of $2\hbar\omega$ and higher excitations into the low-lying spectra, present another challenge for the future.

The difficulties in defining and constructing model spaces that are both adequate and internally consistent coexist with uncertainties about the optimum effective Hamiltonian operator. In the latter context, a major advance would consist of developing techniques to link information about the effective interaction from one mass range (model space) to another. It would also be an important advance to unify the interactions used for Hartree-Fock calculations of closed-shell nuclei with those used for the valence spectra. One of the most successful and commonly used phenomenological interactions for Hartree-Fock calculations is the zero-range density-dependent Skyrme-type interaction. Many of the Skyrme-type parameterizations do not give the correct pairing property when applied to valence spectra, but this problem is corrected with the SGII parameterization (215). Much work remains to be done concerning improvement and unification of effective interactions in nuclei.

To progress further toward the use of more realistic (larger) orbit spaces, better techniques for picking out the important basis states are important, such as those incorporated in the VAMPIRE approach (216) or those implicit in a variety of collective models. With the more conventional techniques discussed here, it is important to push maximum dimensions up by about another order of magnitude, to about 50,000 in the *J-T* scheme or about 1,000,000 in the m scheme. This may be possible with continued improvements of the methods used in the modern codes such as OXBASH (217) or RITSSCHIL (218). Alternatively, perhaps completely new methods will be developed, analogous to the breakthroughs by Whitehead et al (15) and French et al (16).

ACKNOWLEDGEMENTS

This work was supported in part by the US National Science Foundation, grant numbers PHY 87-18772 and 87-14432.

Literature Cited

1. Mayer, M. G., Jensen, J. H. D., *Elementary Theory of Nuclear Structure* New York: Wiley (1955)
2. Ormand, W. E., *Isospin-symmetry violation in light nuclei*, PhD thesis, Mich. State Univ., East Lansing (1986)
3. Brown, B. A., Richter, W. A., Godwin, N. S., *Phys. Rev. Lett.* 45: 1681 (1980)
4. Adelberger, E. G., Haxton, W. C., *Ann. Rev. Nucl. Part. Sci.* 35: 501 (1985)
5. Haxton, W. C., Stephenson, G. J., *Prog. Part. Nucl. Phys.* 12: 409 (1984)

6. Doi, M., Kotani, T., Takasugi, E., *Prog. Theor. Phys. Suppl.* 83: 1 (1985)
7. Brown, B. A., *Nuclear Shell Models*, ed. M. Vallieres, B. H. Wildenthal, p. 42, Singapore: World Sci. (1985)
8. Halbert, E. C., et al., *Adv. Nucl. Phys.* 4: 315 (1971)
9. McGrory, J. B., Wildenthal, B. H., *Ann. Rev. Nucl. Sci.* 30: 383 (1980)
10. Chung, W., *Empirical renormalizations of shell model Hamiltonians and magnetic dipole moments of sd-shell nuclei*, PhD thesis, Mich. State Univ., East Lansing (1976)
11. Ormand, W. E., Brown, B. A., Empirical Isospin-Nonconserving Hamiltonians for Shell-Model Calculations. Preprint (1987)
12. Ormand, W. E., Brown, B. A., *Nucl. Phys.* A440: 274 (1985); and Corrections to Fermi Matrix Elements Superallowed Transitions. Preprint (1988)
13. Ormand, W. E., Brown, B. A., *Phys. Lett.* 174B: 128 (1986)
14. Cohen, S., Kurath, D., *Nucl. Phys.* 73: 1 (1965); *Nucl. Phys.* A101: 1 (1967)
15. Whitehead, R. R., et al., *Adv. Nucl. Phys.* 9: 123 (1977)
16. French, J. B., et al., *Adv. Nucl. Phys.* 3: 193 (1969)
17. Metsch, B. C., Glaudemans, P. W. M., *Z. Phys.* A307: 251 (1982)
18. Kuo, T. T. S., *Ann. Rev. Nucl. Sci.* 24: 101 (1974)
19. Shurpin, J., Kuo, T. T. S., Strottman, D., *Nucl. Phys.* A408: 310 (1983)
20. Kuo, T. T. S., Brown, G. E., *Nucl. Phys.* 85: 40 (1966)
21. Kuo, T. T. S., *Nucl. Phys.* A103: 71 (1967)
22. Wildenthal, B. H., *Prog. Part. Nucl. Phys.* 11: 5 (1984)
23. Brown, B. A., et al., *Ann. Phys.* 182: 191 (1988)
24. Wildenthal, B. H., See Ref. 7, p. 346
25. Ropke, H., et al., *Z. Phys.* A324: 173 (1986)
26. Ropke, H., et al., *Z. Phys.* A324: 187 (1986)
27. Tikkanen, P., et al., *Phys. Rev.* C36: 32 (1987)
28. Watt, R., et al., *J. Phys.* G7: L145 (1981)
29. Poves, A., Retamosa, J., *Phys. Lett.* 184B: 311 (1987)
30. Fifield, L. K., et al., *Nucl. Phys.* A437: 141 (1985)
31. Woods, C. L., et al., *Nucl. Phys.* A437: 454 (1985); A476: 392 (1988)
32. Woods, P. J., et al., *Z. Phys.* A321: 119 (1985)
33. Fifield, L. K., et al., *Nucl. Phys.* A440: 531 (1985)
34. Smith, R. J., et al., *Z.Phys.* A324: 283 (1986)
35. Drumm, P. V., et al., *Nucl. Phys.* A441: 95 (1985)
36. Gillibert, A., et al., *Phys. Lett.* 176B: 317 (1986)
37. Langevin, M., et al., *Nucl. Phys.* A455: 149 (1986)
38. Gillibert, A., et al., *Phys. Lett.* 192B: 39 (1987)
39. Pougheon, F., et al., *Europhys. Lett.* 2: 505 (1986)
40. Viera, D. J., et al., *Phys. Rev. Lett.* 57: 3253 (1986)
41. Woods, P. J., et al., *Phys. Lett.* 182B: 297 (1986)
42. Woods, P. J., et al., *Phys. Lett.* 150B: 79 (1985)
43. Detraz, C., et al., *Nucl. Phys.* A394: 378 (1983)
44. Fifield, L. K., et al., *Nucl. Phys.* A453: 497 (1986)
45. Endt, P.M., *At. Data Nucl. Data Tables* 19: 23 (1977)
46. Brown, B. A., Richter, W. A., Wildenthal, B. H., *J. Phys.* G11: 1191 (1985) (Note that the scale for the matrix elements shown in Fig. 2 of this paper should be reduced by a factor of three and scale for the matrix elements shown in Figs. 3 and 4 should be reduced by a factor of four.)
47. Kirson, M. W., *Phys. Lett.* 47B: 110 (1973)
48. Klingenbeck, K., et al., *Phys. Rev.* C15: 1483 (1977)
49. Yoro, K., *Nucl. Phys.* A333: 67 (1980)
50. Timmer, G. A., et al., *Phys. Lett.* 82B: 305 (1982); Metsch, B. C., et al., *Z. Phys.* A306: 105 (1982)
51. Yoshinada, K., *Phys. Rev.* C26: 1784 (1982)
52. Hosaka, A., Kubo, K. I., Toki, H., *Nucl. Phys.* A444: 76 (1985)
53. Deleted in proof
54. Brown, B. A., Wildenthal, B. H., *Phys. Rev.* C28: 2397 (1983)
55. Wildenthal, B. H., In *Capture Gamma-Ray Spectroscopy and Related Topics*, ed. S. Raman, *AIP Conf. Proc.* 135: 89 (1985)
56. Wildenthal, B. H., In *Weak and Electromagnetic Interactions in Nuclei*, ed. H. V. Klapdor, p. 18. Berlin: Springer-Verlag (1986)
57. Brown, B. A., Wildenthal, B. H., *At. Data Nucl. Data Tables* 33: 347 (1985)
58. Brown, B. A., Wildenthal, B. H., *Nucl. Phys.* A474: 290 (1987)
59. Etchegoyen, M. C., et al., Analysis of Magnetic Dipole Transitions Between sd-shell States. Preprint (1988)

60. Curtin, M. A., et al., *Phys. Rev. Lett.* 56: 34 (1986)
61. Rapaport, J., et al., *Nucl. Phys.* A427: 332 (1984)
62. Wildenthal, B. H., Curtin, M. S., Brown, B. A., *Phys. Rev.* C28: 1343 (1983)
63. Baumann, P., et al., *Phys. Rev.* C36: 765 (1987)
64. Dufour, J. P., et al., *Z. Phys.* A324: 487 (1986)
65. Samuel, M., et al., *Phys. Rev.* C37: 1314 (1988)
66. Deleted in proof
67. Alburger, D. E., Warburton, E. K., *Phys. Rev.* C35: 1479 (1987)
68. Aysto, J., et al., *Phys. Rev.* C32: 1700 (1985)
69. Borrel, V., et al., *Nucl. Phys.* A473: 331 (1987)
70. Müller, W., et al., *Nucl. Phys.* A430: 61 (1984); Bjornstad, T., et al., *Nucl. Phys.* A443: 283 (1985); Borge, M. J. G., et al., *Phys. Scr.* 36: 218 (1987)
71. Aysto, J., Cerny, J., In *Treatise on Heavy-Ion Science*, Vol. 8, ed. D. A. Bromley. New York: Plenum. In press
72. Anderson, B. D., et al., *Phys. Rev.* C27: 1387 (1983)
73. Djalali, C., et al., *Phys. Rev.* C35: 1201 (1987)
74. Rapaport, J., et al., *Nucl. Phys.* A431: 301 (1984)
75. Willis, A., et al., *Nucl. Phys.* A464: 315 (1987)
76. Brown, B. A., Wildenthal, B. H., *Phys. Rev.* C27: 1296 (1983)
77. Sawafta, R., et al., *Phys. Lett.* 201B: 219 (1988)
78. Madey, R., et al., *Phys. Rev.* C35: 2011; C36: 1647 (1987)
79. Anantaraman, N., et al., *Phys. Rev. Lett.* 52: 1409 (1984)
80. Anderson, B. D., et al., *Phys. Rev.* C36: 2195 (1987)
81. Furukawa, K., et al., *Phys. Rev.* C36: 1686 (1987)
82. Hausser, O., et al., *Phys. Rev.* C37: 119 (1988)
83. Sekine, T., et al., *Nucl. Phys.* A467: 93 (1987)
84. Miyatake, H., et al., *Nucl. Phys.* A470: 328 (1987)
85. Anderson, B. D., et al., *Phys. Rev.* C31: 1147, 1161 (1985)
86. Goodman, C. D., Bloom, S. D., *Spin Excitations in Nuclei*, ed. F. Petrovich, G. E. Brown, G. T. Garvey, C. D. Goodman, R. A. Lindgren, W. G. Love, p. 143. New York: Plenum (1984)
87. Alford, W. P., *AIP Conf. Proc.* 150: 710 (1987) and private communication
88. Häusser, O., *AIP Conf. Proc.* 164: 604 (1988)
89. Lederer, C. M., Shirley, V. S., *Table of Isotopes*, Appendix VII. New York: Wiley (1978)
90. Rogers, W. F., et al., *Phys. Lett.* 177B: 293 (1986)
91. Berg, U. E. P., et al., *Phys. Lett.* 140B: 191 (1984)
92. Vodhanel, R., et al., *Phys. Rev.* C35: 921 (1987)
93. Knupfer, W., et al., *Nucl. Phys.* A457: 292 (1986)
94. Towner, I. S., *Phys. Rep.* 155: 264 (1987)
95. Arima, A., et al., *Adv. Nucl. Phys.* 18: 1 (1987)
96. Towner, I. S., Khanna, F. C., *Nucl. Phys.* A399: 334 (1983)
97. Oset, E., Rho, M., *Phys. Rev. Lett.* 42: 47 (1979)
98. Sagawa, H., Lee, T. S. H., Ohta, K., *Phys. Rev.* C33: 629 (1986)
99. Serot, B., Walecka, J. D., *Adv. Nucl. Phys.* 16: 1 (1986)
100. Bouyssy, A., Marcos, S., Mathiot, J. F., *Nucl. Phys.* A415: 497 (1984)
101. Kurasawa, H., Suzuki, T., *Phys. Lett.* 165B: 234 (1985); *Nucl. Phys.* A454: 527 (1986)
102. McNeil, J. A., et al., *Phys. Rev.* C34: 746 (1986)
103. Ichii, S., et al., *Phys. Lett.* 192B: 11 (1987)
104. Blunden, P. G., *Nucl. Phys.* A464: 525 (1987)
105. Delorme, J., Towner, I. S. Preprint (1987)
106. Adelberger, E. G., et al., *Nucl. Phys.* A417: 269 (1984) [More recent M1 data and analyses for the $A = 39$ transitions are given by Alexander, T. K., et al., *Nucl. Phys.* A477: 453 (1988)]
107. Carchidi, M., Wildenthal, B. H., Brown, B. A., *Phys. Rev.* C34: 2280 (1986)
108. Spear, R. H., *Phys. Rep.* 73: 369 (1981)
109. Weber, R., et al., *Nucl. Phys.* A377: 361 (1982)
110. Jeckelmann, B., et al., *Nucl. Phys.* A408: 495 (1983)
111. Sternheimer, R. M., Peierls, R. F., *Phys. Rev.* A4: 1722 (1971)
112. Brown, B. A., Arima, A., McGrory, J. B., *Nucl. Phys.* A277: 77 (1977)
113. Brown, B. A., et al., *Phys. Rev.* C26: 2247 (1982)
114. Alexander, T. K., et al., *Nucl. Phys.* A444: 285 (1985)
115. Alexander, T. K., Castel, B., Towner, I. S., *Nucl. Phys.* A445: 189 (1985)
116. Lappalainen, R., Keinonen, J.,

Luukkainen, A., *Nucl. Phys.* A441: 1 (1985)
117. Morris, C. L., et al., *Phys. Rev.* C35: 1388 (1987)
118. Saha, A., et al., *Phys. Rev. Lett.* 52: 1876 (1984)
119. Saha, A., et al., *Phys. Lett.* 114B: 419 (1982)
120. Alarcon, R., et al., *Phys. Rev.* C31: 697 (1985)
121. Bernstein, A. M., et al., *Phys. Rev. Lett.* 49: 451 (1982)
122. Miskemen, R. A., et al., *Phys. Lett.* 131B: 26 (1983)
123. Brown, V. R., Bernstein, A. M., Madsen, V. A., *Phys. Lett.* 164B: 217 (1983)
124. Brown, B. A., Wildenthal, B. H., *Phys. Rev.* C21: 2107 (1980)
125. Brown, B. A., *Neutron-Nucleus Collisions A Probe of Nuclear Structure*, ed. J. Rapaport, et al., *AIP Conf. Proc.* 124: 183 (1985)
126. Sagawa, H., Brown, B. A., *Phys. Lett.* 150B: 247 (1984)
127. Kuo, T. T. S., Osnes, E., *J. Phys.* G6: 335 (1980)
128. Sagawa, H., Brown, B. A., *Nucl. Phys.* A430: 84 (1984)
129. Brown, B. A., et al., *Phys. Rev.* C32: 1127 (1985)
130. Brown, B. A., Radhi, R., Wildenthal, B. H., *Phys. Rep.* 101: 313 (1983)
131. Blok, H., et al., *Phys. Lett.* 149B: 441 (1984)
132. Wildenthal, B. H., Brown, B. A., Sick, I., *Phys. Rev.* C32: 2185 (1985)
133. Radhi, R., *Calculations of elastic and inelastic electron scattering in light nuclei with shell-model wave functions*, PhD thesis, Mich. State Univ., East Lansing (1983)
134. Ryan, P. J., et al., *Phys. Rev.* C27: 2515 (1983)
135. Donne, A. J. H., et al., *Nucl. Phys.* A455: 453 (1986)
136. Miessen, H., et al., *Nucl. Phys.* A430: 189 (1984)
137. Brown, B. A., Radhi, R., Wildenthal, B. H., *Phys. Lett.* 133B: 5 (1983)
138. Deleted in proof
139. Blunden, P. G., Castel, B., *Nucl. Phys.* A445: 742 (1985)
140. Deleted in proof
141. Knupfer, W., Metsch, B. C., *Phys. Rev.* C27: 2487 (1983)
142. Willis, A., et al., *Nucl. Phys.* A464: 315 (1987)
143. Hino, M., Muto, K., Oda, T., *J. Phys.* G13: 1119 (1987)
144. Chaves, L., Poves, A., *Phys. Rev.* C34: 1137 (1986)
145. Donnelly, T. W., Sick, I., *Rev. Mod. Phys.* 56: 461 (1984)
146. Nolen, J. A., Schiffer, J. P., *Ann. Rev. Nucl. Sci.* 19: 471 (1969)
147. MacGregor, A., Johnston, A., Ewing, J. S., *Nucl. Phys.* A412: 1 (1984)
148. Brown, B. A., Wildenthal, B. H., *Phys. Lett.* 198B: 29 (1987)
149. McGrory, J. B., *Phys. Rev.* C8: 693 (1973)
150. McGrory, J. B., Wildenthal, B. H., *Phys. Lett.* 103B: 173 (1981)
151. Cole, B. J., *J. Phys.* G7: 25, 173 (1981); G11: 953; G11: 961 (1985)
152. van Hees, A. G. M., Glaudemans, P. W. M., *Z. Phys.* A303: 267 (1981)
153. Mooy, R. B. M., Glaudemans, P. W. M., *Z. Phys.* A312: 59 (1983)
154. Yokoyama, A., Horie, H., *Phys. Rev.* C31: 1012 (1985)
155. Mooy, R. B. M., Glaudemans, P. W. M., *Z. Phys.* A319: 343; A318: 245 (1984); *Nucl. Phys.* A438: 461 (1985)
156. Muto, K., Horie, H., *Phys. Lett.* 138B: 9 (1984); *Nucl. Phys.* A440: 254 (1985)
157. Muto, K., *Nucl. Phys.* A451: 481 (1986)
158. Liu, H., Zamick, L., *Phys. Rev.* C36: 2064 (1987)
159. Metsch, B. C., Glaudemans, P. W. M., *Nucl. Phys.* A352: 60 (1981)
160. Vennink, R., *Z. Phys.* A294: 241 (1980)
161. Glaudemans, P. W. M., Vennink, R., *Phys. Lett.* 95B: 171 (1980)
162. van Hees, A. G. M., Glaudemans, P. W. M., Metsch, B. C., *Z. Phys.* A293: 327 (1979)
163. Eulenberg, G., et al., *Phys. Lett.* 116B: 113 (1982)
164. Poves, A., Zuker, A., *Phys. Rep.* 70: 235 (1981)
165. Ji, X., Wildenthal, B. H., *Phys. Rev.* C37: 1256 (1988)
166. Oxorn, K., et al., *Z. Phys.* A321: 485 (1985)
167. Blomqvist, J., Rydstrom, L., *Phys. Scripta* 31: 31 (1985)
168. Raghavan, P., et al., *Phys. Rev. Lett.* 54: 2592 (1985)
169. Amusa, A., Lawson, R. D., *Z. Phys.* A307: 333 (1982); A314: 205 (1983)
170. Amusa, A., *Z. Phys.* A322: 567 (1985)
171. Chiang, H. C., Wang, M. C., Han, C. S., *J. Phys.* G6: 345 (1980)
172. Muto, K., Shimano, T., Horie, H., *Phys. Lett.* 135B: 349 (1984)
173. Muto, K., et al., *Phys. Lett.* 165B: 25 (1985)
174. Momoki, G., Ogawa, K., Tonozuka, I., *INS-Rep.*-563, Dec. (1985)
175. Prade, H., et al., *Nucl. Phys.* A425: 317 (1984)

176. Kruse, H. G. W., Wildenthal, B. H., *Bull. Am. Phys. Soc.*27: 725 (1982)
177. Berant, Z., et al., *Phys. Rev.* C31: 570 (1985)
178. Sagawa, H., et al., *Nucl. Phys.* A462: 1 (1987)
179. Blomqvist, J., Kleinheinz, P., Daley, P. J., *Z. Phys.* A312: 26 (1983); Chung, Y. H., et al., *Phys. Rev.* C29: 2153 (1984)
180. Horn, D., et al., *Phys. Rev. Lett.* 50: 1447 (1983)
181. Yates, S. W., *Z. Phys.* A324: 417 (1986)
182. Lawson, R., *Z. Phys.* A303: 51 (1981)
183. Helppi, H., et al., *Phys. Lett.* 115B: 11 (1982)
184. Poletti, A. R., et al., *Nucl. Phys.* A359: 180 (1981)
185. Muto, K., Oda, T., Horie, H., *Phys. Lett.* 118B: 261 (1982)
186. Lonnroth, T., et al., *Phys. Rev.* C27: 180 (1983)
187. Zwarts, D., Glaudemans, P. W. M., *Z. Phys.* A320: 487 (1985)
188. van Ruyven, J. J., et al., *Nucl. Phys.* A449: 579 (1986)
189. Gloeckner, D. H., Lawson, R. D., *Phys. Lett.* 53B: 313 (1974)
190. McGrory, J. B., Wildenthal, B. H., *Phys. Lett.* 60B: 5 (1975)
191. Ceuleneer, R., Vandepeutte, P., Semay, C., *Phys. Lett.* 196B: 303 (1987)
192. Bevelacqua, J. J., *Phys. Rev.* C33: 699 (1986)
193. Millener, D. J., Kurath, D., *Nucl. Phys.* A255: 315 (1975)
194. Millener, D. J., et al., *Phys. Rev.* C26: 1167 (1982)
195. Millener, D. J., *Phys. Rev.* C28: 497 (1983)
196. Warburton, E. K., Alburger, D. E., Millener, D. J., *Phys. Rev.* C29: 2281 (1984)
197. Hicks, R. S., et al., *Phys. Rev.* C30: 1 (1984)
198. Blilie, C. L., et al., *Phys. Rev.* C30: 1989 (1984)
199. Seestrom-Morris, S. J., et al., *Phys. Rev.* C31: 923 (1985)
200. Hicks, R. S., et al., *Phys. Rev.* C34: 1161 (1986)
201. Chakravarti, S., et al., *Phys. Rev.* C35: 2197 (1987)
202. Millener, D. J., *Phys. Rev.* C36: 1643 (1987)
203. van Hees, A. G. M., Glaudemans, P. W. M., *Z. Phys.* A314: 323; A315: 223 (1983) [See also Poppelier, N. A. F., et al., *Phys. Lett.* 157B: 120 (1985)]
204. van Hees, A. G. M., Wolters, A. A., Glaudemans, P. W. M., *Phys. Lett.* 196B: 19 (1987); *Nucl. Phys.* A476: 61 (1988)
205. Warburton, E. K., et al., *Phys. Rev.* C34: 1031 (1986)
206. Warburton, E. K., *Phys. Rev.* C35: 2278 (1987)
207. Warburton, E. K., Becker, J. A., *Phys. Rev.* C35: 1851 (1987)
208. Olness, J. W., et al., *Phys. Rev.* C34: 2049 (1986)
209. Woods, C. L., *Nucl. Phys.* A451: 413 (1986)
210. Snover, K. A., et al., *Phys. Rev.* C27: 1837 (1983)
211. Wolters, A. A., van Hees, A. G. M., Glaudemans, P. W. M., *Europhys. Lett.* 5: 7 (1988)
212. Reehal, B. S., Wildenthal, B. H., *Part. Nucl.* 6: 137 (1973); McGrory, J. B., Wildenthal, B. H., *Phys. Rev.* C7: 974 (1973)
213. Hseih, S. T., Mooy, R. B. M., Wildenthal, B. H., *Nuclear Structure at High Spin, Excitation, and Momentum Transfer*, ed. H. Nann, *AIP Conf. Proc.* 142: 357 (1986)
214. Chaves, L., Poves, A., *Phys. Lett.* 171B: 343 (1986)
215. Sagawa, H., Brown, B. A., Scholten, O., *Phys. Lett.* 159B: 228 (1985)
216. Schmid, K. W., Grummer, F., Faessler, A., *Ann. Phys.* 180: 1 (1987)
217. Etchegoyen, A., et al., *MSU-NSCL Rep.* 524 (1985)
218. Zwarts, D., *Comput. Phys. Commun.* 38: 365 (1985)
219. MacFarlane, M. H., *Phys. Lett.* 182B: 265 (1986)
220. Hino, M., et al., *Phys. Rev.* C37: 1328 (1988)